Optimization of Novel Air-to-Refrigerant Heat Exchangers for Lower-GWP Refrigerants in Air-Conditioning Systems

James Tancabel[a], *Vikrant* Aute[b], *Jiazhen* Ling[c]

[a]PhD Candidate, Center for Environmental Energy Engineering, Department of Mechanical Engineering, University of Maryland, College Park, Maryland, USA. jmtanc@umd.edu.

[b]Research Scientist & Co-Director, Center for Environmental Energy Engineering, Department of Mechanical Engineering, University of Maryland, College Park, Maryland, USA. vikrant@umd.edu.

[c]Associate Research Professor, Center for Environmental Energy Engineering, University of Maryland, College Park, Maryland, USA. jiazhen@umd.edu.

Abstract. Air-to-refrigerant heat exchangers (HXs) are fundamental components in HVAC&R systems, and considerable research has focused on reducing the airside thermal resistance, which can exceed 70-90% of the overall resistance. Traditional HX design ideology utilizes secondary heat transfer surfaces (fins) to reduce the airside thermal resistance by increasing the airside heat transfer area. However, fins also have inherent deficiencies such as increased airside pressure drop, material costs, and HX fouling/frosting potential. Recent advancements in simulation tools such as Computational Fluid Dynamics (CFD) and Finite Element Analysis (FEA) and also in optimization algorithms have enabled researchers to apply shape and topology optimization to the primary heat transfer surfaces (e.g., tubes) to design high performance, highly compact HXs which do not require fins. These novel HXs feature reduced size, weight, cost, and refrigerant charge compared to current state-of-the-art HXs while maintaining or improving system-level performance, thereby reducing the overall environmental impact. Such factors are especially important given the recent governmental and industrial shifts to low-GWP flammable and mildly-flammable refrigerants, which have highly regulated charge amounts. In this paper, an HX optimization framework featuring automated CFD and FEA simulations and approximation-assisted optimization is utilized to optimize a residential A/C condenser for three different refrigerants: (i) R410A (industry-standard for US residential A/C units), (ii) R32 (most popular lower-GWP replacement for R410A in the EU), and (iii) R454B (another lower-GWP alternative to R410A). Preliminary findings show that the optimal HXs achieve at least 20% reductions in airside pressure drop and envelope volume, up to 11% reduction in tube material volume, and more than 40% reduction in tube internal volume while delivering similar capacity to the state-of-the-art baseline HX. The differences between the refrigerant-specific optimal HXs are also discussed in detail to shed light on how the refrigerant choice impacts the final HX designs. By using systematic optimization, it is possible to arrive at highly compact and lighter HX designs for any of the new lower-GWP replacement refrigerants.

Keywords. heat exchanger, optimization, low-GWP, R32, R454B.
DOI: https://doi.org/10.34641/clima.2022.245

1. Introduction

Air-to-refrigerant heat exchangers (HXs) are fundamental components in all HVAC&R systems. Compact HXs, i.e., HXs with tube characteristic diameters smaller than 6.0 mm [1], are of particular interest to researchers since their intrinsically high heat transfer area to envelope volume ratio can yield significant size reductions. However, these small characteristic diameter tubes do not have adequate primary heat transfer area to achieve the required thermal resistance to satisfy the HX capacity requirements. Thus, compact HXs typically utilize fins to increase the airside heat transfer area and satisfy the thermal resistance requirements. However, fins have inherent drawbacks including increased airside pressure drop, material consumption, and fouling/frosting potential. Recent

research [2] has noted that as characteristic diameter decreases, finless surfaces have superior airside thermal-hydraulic performance compared to similarly-sized finned surfaces. Additionally, small diameter, round tube HXs have been well-studied throughout the literature [3-6].

More recently, Bacellar et al. [2,7] argued that classical HX design paradigms should evolve to leverage modern computational and manufacturing capabilities. To this end, the authors developed a comprehensive multi-scale analysis and shape and topology optimization framework capable of designing finless compact HXs which utilize novel, small diameter, non-round tubes. Their methodology was experimentally validated using an additively manufactured proof-of-concept HX design, further strengthening the case for implementing shape optimization and additive manufacturing into HX design ideology.

In a related work, Radermacher et al. [8] suggested that non-round, shape-optimized tube designs may lack the required mechanical strength for pressure-holding, thereby requiring detailed structural analyses to verify pressure-holding capabilities of all candidate geometries. Additionally, Tancabel et al. [9] noted that no air-to-refrigerant HX shape and topology optimization studies explicitly considered tube mechanical strength.

In this paper, we present the application of an HX design optimization methodology which features integrated multi-scale and multi-physics analyses and shape and topology optimization [10-11] to optimize a residential air-conditioning (A/C) unit condenser using novel, shape-optimized non-round tubes which can be conventionally (i.e., non-additively) manufactured. We consider three different refrigerants: (i) R410A (GWP = 2,088), the industry-standard for US residential A/C units, (ii) R32, a lower-GWP (GWP = 677) alternative to R410A which is the most popular replacement for R410A in the EU [12-16], and (iii) R454B, an even lower-GWP (GWP = 466) alternative to R410A (compared to R32) [16-19]. Comparisons between the optimal HX designs for each refrigerant are discussed in detail to shed light on how the refrigerant choice impacts the final HX design.

2. Methodology

2.1 Design Optimization Framework

The HX design optimization framework (Fig. 1) utilizes Approximation-Assisted Optimization (AAO) [20] involving automated Computational Fluid Dynamics (CFD) [21] and Finite Element Analysis (FEA) simulations [10-11], Kriging metamodels [22], and optimization with a multi-objective genetic algorithm (MOGA) [23].

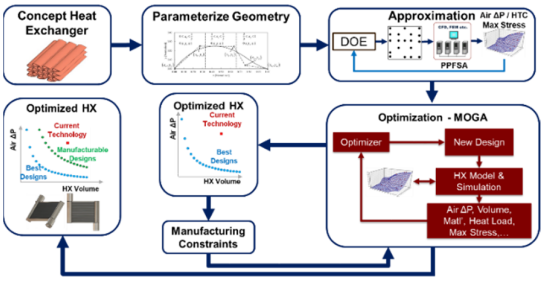

Fig. 1 – Numerical optimization framework.

2.2 Problem Description

High performance HXs featuring novel, non-round tubes have been investigated for many applications [10-11, 24]. In this research, the optimization framework is utilized to design novel, finless, air-to-refrigerant condensers for residential A/C applications using lower-GWP alternative refrigerants. The baseline HX is a commercially-available, state-of-the-art nominal 5.28 kW (1.5-Ton) tube-fin air-to-R410A condenser. Three refrigerants are investigated: (i) R410A, (ii) R32, and (iii) R454B. The inlet conditions for each refrigerant are taken from commercially-available residential A/C units with nominal 5.28 kW (1.5-Ton) capacity [25]. Sample schematics for a representative tube-fin HX and a finless HX with shape-optimized tubes are shown in Figure 2.

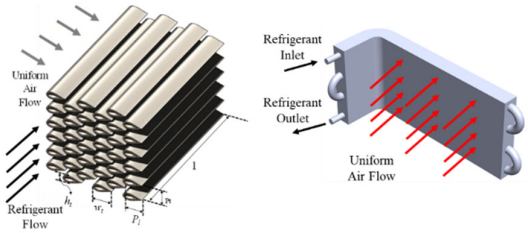

Fig. 2 – (Left) Generic HX with shape-optimized tubes; (Right) Generic multi-pass tube-fin condenser.

The HXs are in cross-flow, and all HX models assume the following: (i) uniform normal inlet air velocity on the HX face, and (ii) fully-developed, uniform refrigerant flow. The airside thermal-hydraulic performance is predicted using CFD, and the tube-level mechanical performance is computed using FEA. Refrigerant-side performance is computed using existing correlations for single and two-phase flow in small diameter channels.

The framework utilizes fourth-order Non-Uniform Rational B-Splines (NURBS) [26] to represent the novel, non-round tube shapes (Fig. 3). The tube shape considered herein [2] has been conventionally manufactured in both copper and aluminum. Burst pressure testing and FEA modelling of the copper tubes showed minimal deformation up to 20.0 MPa, validating the tube structural strength [27]. We therefore consider the copper version herein.

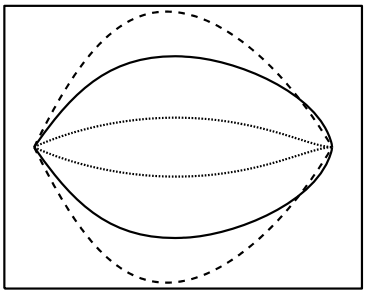

Fig. 3 – Sample non-round tube shapes.

2.3 Parallel Parameterized Fluid & Structural Analysis

It is impractical to simulate an entire multi-variable Design of Experiments (DoE) manually, and thus the entire simulation process must be automated to reduce the computational time burden. To this end, Abdelaziz et al. [21] developed Parallel Parameterized CFD (PPCFD) to automate CFD simulations, resulting in more than 90% engineering time savings. Similarly, Tancabel et al. [10-11] integrated automated FEA simulations into the PPCFD framework for use in multi-physics analyses of HXs utilizing shape and topology optimized tubes. Their framework was termed Parallel Parameterized Fluid & Structural Analysis (PPFSA).

As mentioned above, the modelling and experimental validation of the copper tube structural integrity eliminates the need to consider the structural component of PPFSA. Thus, it is only necessary to consider the CFD component of PPFSA, which is explained in detail in the following sections. All present analyses utilize the ANSYS® 18.0 platform [28-29]. Geometry and meshing are performed using Gambit® 2.4.6 [28], and all CFD simulations are run using Ansys® Fluent 18.0 [29].

2.4 CFD Modelling, Post-Processing, & Uncertainty Analysis

The airside CFD computational domain (Fig. 4) is a two-dimensional cross-section of the HX in the depth-wise direction wherein all end effects are negligible and the working fluid is dry air. In the near-wall region, an inflation layer mesh is employed with a growth ratio of 1.2 to more accurately capture the boundary layer physics. The core mesh is a pave mesh scheme where the average element size is equal to the last row of the inflation layer.

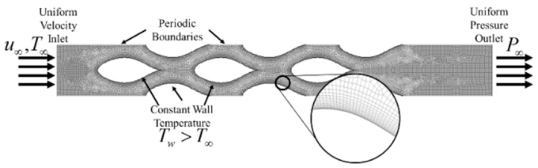

Fig. 4 – Sample CFD domain, mesh, & boundary conditions.

The left boundary is a uniform velocity and temperature inlet, and the right boundary is a uniform atmospheric pressure outlet. The tube walls are fixed to a constant temperature, and periodic boundaries are applied at the upper and lower domain boundaries. The dry air thermophysical properties are computed using polynomial curve fits as a function of temperature, while the density is computed using the ideal gas law. The realizable k-ε (RKE) model [30] is utilized to model turbulence. The convergence criteria utilized is maximum residuals, and the limits are set to 1E-05 for continuity and momentum, 1E-06 for energy, and 1E-03 for turbulence. If these convergence criteria are not met, but the simulation stabilizes to a solution, the simulation is considered converged if the standard deviation of the final 100 iterations is less than 0.5% of the average of those same 100 iterations.

The CFD simulations are utilized to determine the airside thermal-hydraulic performance only, and thus the wall and refrigerant thermal resistances can be neglected. This allows for the airside heat transfer coefficient to be easily computed using UA-Log Mean Temperature Difference (UA-LMTD) method as given in equation (1) [31], while the airside pressure drop is computed as the difference between the inlet and outlet static pressures as given in equation (2).

$$h_{air} = \frac{\dot{m} c_p}{A_w} \cdot \ln\left[\frac{T_w - T_{in}}{T_w - T_{out}}\right] \quad (1)$$

$$\Delta P_{air} = P_{in} - P_{out} \quad (2)$$

The CFD modelling grid resolution uncertainty is quantified using the Grid Convergence Index (GCI) method [32-35] for all boundary designs using three grid resolutions and a constant refinement ratio of 1.3. The GCI for a given design is computed using the absolute relative difference for a metric of interest (in this case, h_{air} and ΔP_{air}) between two consecutive grid sizes [34-35]. All CFD uncertainty quantification results are tabulated in Table 1.

Tab. 1 – CFD uncertainty quantification using GCI.

Metric	h_{air}	ΔP_{air}
Designs with GCI ≤ 10%	96%	91%
Max	16.5%	54.6%
Average	0.9%	1.25
Median	2.0%	3.3%

2.5 Metamodeling

If a new CFD simulation were required for each individual generated by the optimizer during a single optimization run, tens of thousands of CFD simulations would be required. To reduce this computational burden, this research employs approximation-assisted optimization [20], wherein a simplified model, sometimes called a metamodel, which is capable of accurately representing the simulation behaviour is utilized to carry out the optimization. In this case, metamodels are utilized to

quickly and efficiently compute the airside thermal-hydraulic performance.

A 5000-sample Design of Experiments (DoE) generated using Latin Hypercube Sampling (LHS) [36] was simulated using PPFSA, and Kriging metamodels [22] were built using 2673 converged samples. The metamodels were then verified by comparing the predicted (metamodel) responses to simulated (CFD) responses for 544 converged random samples. The Metamodel Acceptance Score (MAS) [37] was utilized to quantify the metamodel accuracy. The MAS gives the percentage of predicted responses whose absolute relative error compared to the simulated response is less than a prescribed threshold. The metamodel verification results are summarized in Table 2 and Figure 5.

Tab. 2 – Metamodel verification statistics.

Metric	h_{air}	ΔP_{air}
Mean Absolute Error	6.30	14.27
Root Mean Square Error	13.51	41.70
MAS (10%)	97.97%	70.95%
MAS (20%)	99.26%	90.99%

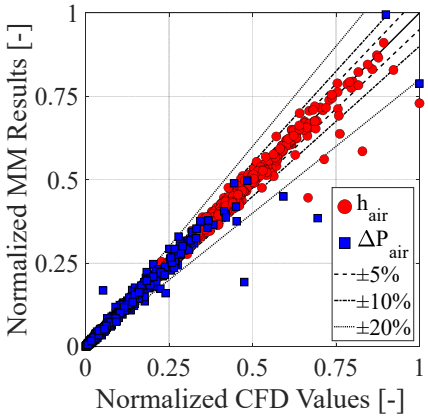

Fig. 5 – Metamodel verification results.

2.6 Multi-Objective Optimization

This research presents the application of a multi-scale and multi-physics analysis with shape and topology optimization methodology [2,7,10-11] which leverages a Multi-Objective Genetic Algorithm (MOGA) [23] to model full HXs with novel tube shapes and topologies. Full HX models are built and simulated using an in-house, experimentally-validated air-to-refrigerant HX modelling tool [39]. CFD-based metamodels are utilized to predict the airside thermal-hydraulic performance (h_{air}, ΔP_{air}). Refrigerant-side thermal-hydraulic performance is evaluated using empirical correlations for single-phase flow and (condensing) two-phase flow in small channels (Tab. 3). Refrigerant thermodynamic property calculations utilize NIST REFPROP v10.0 [39] augmented with polynomial curve fits as proposed by Aute and Radermacher [40].

Tab. 3 – Thermal-hydraulic performance correlations.

Operating Mode	h_{ref} Correlation	ΔP_{ref} Correlation
Air	CFD Metamodels	
Liquid refrigerant	Gnielinski (1976) [41]	Churchill (1977) [42]
Two-phase refrigerant	Shah (2019) [43]	Xu-Fang (2013) [44]
Vapor refrigerant	Gnielinski (1976) [41]	Churchill (1977) [42]

3. Optimization Results & Discussion

3.1 Optimization Problem Formulation

This research considers a bi-objective optimization problem as defined in equation (3) where the objectives are to minimize airside pressure drop and HX core envelope volume. The overall objective is to design air-to-refrigerant condensers featuring the novel non-round tube shape which was conventionally manufactured in copper as discussed above [25, 27] for three different refrigerants: (i) R410A, (ii) R32, and (iii) R454B. For each refrigerant, the inlet air (temperature, volume flow rate) and refrigerant states (temperature, pressure, mass flow rate) are fixed to that of commercially-available residential units with nominal 5.28 kW (1.5-Ton) capacity [25].

$$\begin{aligned} &\min \Delta P_{air}, V_{HX} \\ &\text{s.t.} \\ &\Delta P_{air} \le 2.0 \cdot \Delta P_{air,BL} \quad V_{HX} \le V_{HX,BL} \\ &0.5 \le H_{HX} / L_{HX} \le 2.0 \quad A_f \le A_{f,BL} \\ &\Delta T_{SC,BL} - 1.0\,\text{K} \le \Delta T_{SC} \le \Delta T_{SC,BL} \end{aligned} \tag{3}$$

All optimal HXs have a 60%/40% two-fluid-pass configuration, i.e., the first fluid pass contains 60% of the tubes, and the second fluid pass contains the remaining tubes. The airside pressure drop cannot exceed two times the baseline value, and the HX frontal area cannot exceed the baseline value. Moreover, the HX frontal aspect ratio (height-to-length ratio) is constrained such that the HX is no more than two times as tall as it is long or vice versa. The HX capacity constraint is considered by constraining the condenser outlet subcooling to be at least the same, but no more than 1.0 K more, compared to the baseline value. Note that the problem statement is sufficiently general, and it is possible to find additional promising designs by examining other pass configurations and removing the HX face area constraint. In total, five (5) design variables are considered: tube horizontal spacing, tube vertical spacing, number of tube banks, number of tubes per bank, and inlet air velocity.

Five separate optimization runs are conducted for each refrigerant (R410A, R32, & R454B). The optimal designs presented in the following sections are the

non-dominated set of designs found by combining the output from all optimization runs (for each refrigerant separately) and conducting non-dominated sorting to find the best designs for each refrigerant respectively. Additional MOGA settings are summarized in Table 4.

Tab. 4 – MOGA settings.

Type	Unit	Value
Optimization runs per refrigerant	-	5
Population size	-	50
Replacement	%	20
Iterations	-	300

3.2 Optimization Results

Figures 6 – 8 present a summary of the optimization results coloured by HX face area (Fig. 6), core material volume (Fig. 7), and core internal volume (Fig. 8). All metrics are normalized with respect to the baseline, and the dashed lines represent the 20%-20% improvement region for each objective. For the baseline airside pressure drop, the optimal designs for each refrigerant can achieve ~46% reduction in HX core envelope volume, ~30% reduction in HX face area, ~7% in tube material volume, and ~50% reduction in tube internal volume. For the baseline HX core envelope volume, the optimal designs for each refrigerant can achieve ~46% reduction in airside pressure drop, ~9% reduction in HX face area, and ~20% reduction in tube internal volume. However, for those designs, the tube material volume is ~27% greater than the baseline, which would result in significantly higher manufacturing costs. From an environmental standpoint, the significant tube internal volume reductions will correspond to significant charge reductions and thus lower the overall environmental impact, while the significant face area reductions are highly advantageous to HX manufacturers since face area is directly related to system footprint [25]. These results clearly emphasize that by using systematic optimization, we can arrive at highly compact and lighter HX designs for any of the new lower-GWP replacement refrigerants.

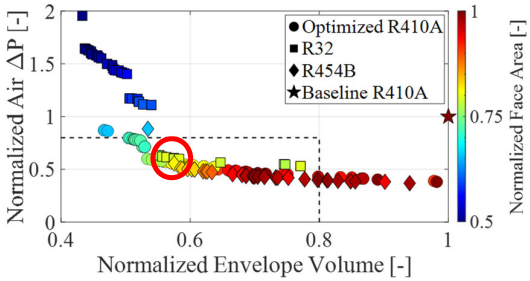

Fig. 6 – Optimization results (Colour: face area).

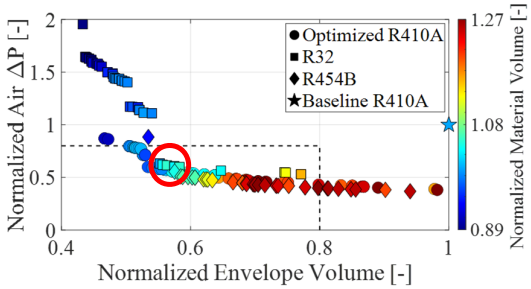

Fig. 7 – Optimization results (Colour: material volume).

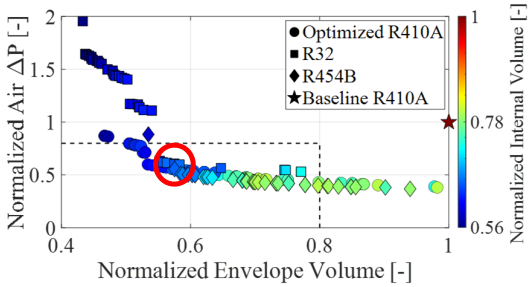

Fig. 8 – Optimization results (Colour: internal volume).

3.3 Comparison of Optimal Designs for each Refrigerant

It is of interest to directly compare the optimal HX designs from each refrigerant case to one another to gain valuable insights into whether, and if so, to what extent, the refrigerant's unique thermophysical properties impact the final HX designs. First, consider the entire set of optimal designs for each refrigerant as a whole. The similarities and differences in across the optimal designs are listed below:

- All HXs have very similar tube pitches and numbers of tube banks, resulting in all HXs having similar airside pressure drops and HX core depths.
  - All R410A and R454B HXs have 4 tubes banks.
  - Most R32 HXs have 5 tube banks, the rest have 4 tube banks.
- On average, R32 HXs have the fewest tubes per bank, while R454B HXs have the most.
  - This could be the result of R32 HXs having more tube banks, which then requires fewer tubes per bank to achieve the desired capacity.
  - Fewer tubes per bank reduces the HX core height, resulting in the R32 HXs having the smallest face areas. Because the air volume flow rate is fixed, the R32 HXs have large inlet air velocities, which could lead to undesirable fan noise / tube aeroacoustics challenges.

Next, we consider three HX designs (one design per refrigerant) as highlighted with red circles in Figures 6 – 8. Note that these HXs were chosen since they are all close together in the objective space (~40% reductions in both HX core envelope volume and

airside pressure drop). The normalized values of different performance metrics for these HXs are highlighted in Table 5, and additional normalized values of HX geometry are listed in Table 6. As mentioned above, all HXs have the same tube shape and similar tube pitches, and thus these values are not listed.

Tab. 5 – Comparison of normalized performance metrics for three optimal HX designs. All values are normalized with respect to the baseline R410A HX.

Fluid	V_{HX}	ΔP_{air}	A_f	V_{Mat}	V_{Int}	Charge
R410A	0.58	0.56	0.81	1.04	0.65	0.63
R32	0.57	0.60	0.79	1.03	0.65	0.52
R454B	0.58	0.56	0.81	1.04	0.65	0.55

Tab. 6 – Comparison of normalized HX geometry values for three optimal HX designs. All values are normalized with respect to the optimal R410A HX.

Fluid	*Number of tube banks*	*Number of tubes per bank*	H_{HX}	L_{HX}
R410A	1.0	1.0	1.0	1.0
R32	1.0	0.73	0.71	1.36
R454B	1.0	0.97	0.97	1.04

It is clear from Tables 5 and 6 that, while the HXs have very similar performance metrics, the HXs themselves are quite different. First and foremost, the R32 and R454B HXs have 15-20% lower refrigerant charge compared to the R410A HX, which is especially advantageous given that R32 and R454B are mildly flammable refrigerants. Additionally, as noted above, the R32 HX has much fewer tubes per bank, but this is compensated by having ~36% longer tubes compared to the R410A HX, while the R454B HX is almost identical to the R410A HX. Looking from a strictly HX standpoint, i.e., assuming that all other system components (e.g., compressor, flammability considerations, etc.) are changed to enable the use of R32 and R454B, the following conclusions can be drawn:

- R32 should not be used as a direct drop-in replacement to R410A HXs. Instead, HX optimization should be done specifically for R32.
- R454B could serve as a near drop-in replacement to R410A in HXs originally designed for R410A.
    - Soft optimization methods (component selection, operating condition tuning, etc.) could be sufficient to efficiently transition R410A HXs to R454B.

4. Conclusions

This paper presents the application of a multi-scale, multi-physics analysis and tube shape and topology optimization methodology, which is utilized to design residential A/C unit condensers for three different refrigerants: (i) R410A and two lower-GWP alternatives (ii) R32, and (iii) R454B. The novel, non-round, shape-optimized tube geometry considered herein has been conventionally manufactured. The optimal HX designs deliver the same capacity as a state-of-the-art baseline tube-fin condenser while achieving at least 20% reductions in airside pressure drop and envelope volume, up to 11% reduction in tube material volume, and more than 40% reduction in tube internal volume, thus showcasing the viability of tube shape and topology optimization for the design of HXs using alternative refrigerants. Detailed comparisons of optimal HXs designs for each refrigerant were also presented, and it was found that the R32 HX geometries showed many differences compared to the R410A HXs, while the R454B and R410A HX geometries were largely similar. This suggests that when considering R32 to replace R410A, separate HX optimization studies may be required to ensure that the HXs are delivering the desired performance. On the other hand, R454B could serve as a near drop-in replacement in HXs originally designed for R410A so long as appropriate soft-optimization techniques such as component selection and operating condition tuning are also considered. In summary, this study highlights how systematic optimization can result in highly compact and lighter HX designs for any of the new lower-GWP replacement refrigerants.

5. Nomenclature

A_f	[m^2]	HX face area
c_p	[$Jkg^{-1}K^{-1}$]	Specific heat
GCI	[-]	Grid convergence index
GWP	[-]	Global warming potential
h	[$Wm^{-2}K^{-1}$]	Heat transfer coefficient
H_{HX}	[m]	HX core height
L_{HX}	[m]	HX core length
$\dot{m}$	[kgs^{-1}]	Mass flow rate
P	[Pa]	Pressure
T	[K]	Temperature
u	[ms^{-1}]	Fluid velocity
$\dot{V}$	[m^3s^{-1}]	Volumetric flow rate
V	[m^3]	Volume
ΔP	[Pa]	Pressure drop
ΔT_{SC}	[K]	Refrigerant subcooling
Subscripts		
air		Air
BL		Baseline
HX		Heat exchanger
in		Inlet
int		Internal
mat		Material
out		Outlet
ref		Refrigerant
w		Wall

6. Acknowledgement

This material is based upon work supported by the U.S. Department of Energy's Office of Energy Efficiency and Renewable Energy under the Building Technologies Office Award Number DE-EE0008221. The views expressed herein do not necessarily represent the views of the U.S. Department of Energy or the United States Government. This work was also supported in part by the Modeling & Optimization

Consortium at the Center for Environmental Energy Engineering at the University of Maryland.

7. Data Access Statement

The datasets generated during and/or analysed during the current study are not publicly available due to the on-going nature of the research project, but the authors will make every reasonable effort to publish them in near future upon project completion.

8. References

[1] Kays, W. & London, A., Compact Heat Exchangers, 1984; McGraw-Hill, New York.

[2] Bacellar, D., Aute, V., Huang, Z., & Radermacher, R. Design optimization and validation of high-performance heat exchangers using approximation assisted optimization and additive manufacturing. Science & Technology for the Built Environment, 2017; 23(6): 896-911.

[3] Paitoonsurikarn, S., Kasagi, N., & Suzuki Y. Optimal design of micro bare-tube heat exchanger. Symposium on Energy Engineering, 2000; 972–979: Hong Kong, China.

[4] Saji, N., Nagai, S., Tsuchiya, K., Asakura, H., & Obata, M, Development of a compact laminar flow heat exchanger with stainless steel micro-tubes. Physica C, 2001; 354(1-4): 148-151.

[5] Kasagi, N., Suzuki, Y., Shikazono, N., & Oku, T. Optimal design and assessment of high performance micro bare-tube heat exchangers. 4th International Conference Compact Heat Exchangers and Enhancement Technologies for the Process Industries, 2003; 241-246: Crete, Greece.

[6] Chen, H.T., Lin, Y.S., Chen, P. C., & Chang, J.R. Numerical and experimental study of natural convection heat transfer characteristics for vertical plate fin and tube heat exchangers with various tube diameters. International Journal of Heat & Mass Transfer, 2016; 100: 320-331.

[7] Bacellar, D., Huang, Z., Tancabel, J., Aute, V., & Radermacher, R. Multi-scale analysis, shape optimization and experimental validation of novel air-to-refrigerant heat exchangers, 9th World Conference on Experimental Heat Transfer, Fluid Mechanics, and Thermodynamics, 2017; Iguazu Falls, Brazil.

[8] Radermacher, R., Bacellar, D., Aute, V., Huang, Z., Hwang, Y., Ling, J., Muehlbauer, J., Tancabel, J., Abdelaziz, O., & Zhang, M. Miniaturized Air-to-Refrigerant Heat Exchangers, 2017; United States Department of Energy Report for Project Award DE-EE0006114.

[9] Tancabel, J., Aute, V., & Radermacher, R. Review of Shape and Topology Optimization for Design of Air-to- Refrigerant Heat Exchangers. 17th International Refrigeration and Air Conditioning Conference, Purdue University, 2018; Paper 1965: West Lafayette, Indiana, USA.

[10] Tancabel, J., Aute, V., Ling, J., & Radermacher, R. Multi-scale and multi-physics analysis of novel high performance, reduced charge evaporators with novel tube shapes. 9th International Conference on Compressor and Refrigeration, 2019; Xi'an, China.

[11] Tancabel, J., Aute, V., Ling, J., & Radermacher, R. Design optimization of high performance, reduced charge condensers with novel tube shapes. 25th International Congress of Refrigeration, 2019; Montreal, Quebec, Canada.

[12] Li, H. By, R. System Soft-Optimization Tests of Refrigerant R-32 in a 3-ton Split System Air-Conditioner. Air-Conditioning, Heating, and Refrigeration Institute (AHRI) Low-GWP Alternative Refrigerants Evaluation Program (Low-GWP AREP) Test Report #32; 2015.

[13] Alabdulkarem, A., Eldeeb, R., Hwang, Y., Aute, V., & Radermacher, R. Testing, simulation and soft-optimization of R410A low-GWP alternatives in heat pump system. International Journal of Refrigeration, 2015; 60: 106-117.

[14] Mota-Babiloni, A., Navarro-Esbrí, J., Makhnatch, P., & Molés, F. Refrigerant R32 as lower GWP working fluid in residential air conditioning systems in Europe and the USA. Renewable and Sustainable Energy Reviews, 2017; 80: 1031-1042.

[15] Heredia-Aricapa, Y., Belman-Flores, J.M., Mota-Babiloni, A., Serrano-Arellano, J., & García-Pabón, J.J. Overview of low GWP mixtures for the replacement of HFC refrigerants: R134a, R404A and R410A. International Journal of Refrigeration, 2020; 111: 113-123.

[16] Nair, V. HFO refrigerants: A review of present status and future prospects. International Journal of Refrigeration, 2021; 122: 156-170.

[17] Panato, V.H., Pico, D.F.M., & Bandarra Filho, E.P. Experimental evaluation of R32, R452B and R454B as alternative refrigerants for R410A in a refrigeration system. *International Journal of Refrigeration*, 2021.

[18] Shen, B., Li, Z., & Gluesenkamp, K.R. Experimental study of R452B and R454B as drop-in replacement for R410A in split heat pumps having tube-fin and microchannel heat exchangers. *Applied Thermal Engineering*, 2021; 204: 117930.

[19] Sieres, J., Ortega, I., Cerdeira, F., & Álvarez, E. Drop-in performance of the low-GWP alternative refrigerants R452B and R454B in an R410A liquid-to-water heat pump. *Applied Thermal Engineering*, 2021; *182*: 116049.

[20] Simpson, T. W., Poplinski, J. D., Koch, P. N., & Allen, J. K. Metamodels for computer-based engineering design: survey and recommendations. Engineering with computers, 2001;17(2): 129-150.

[21] Abdelaziz, O., Aute, V., Azarm, S., & Radermacher, R., Approximation-assisted optimization for novel compact heat exchanger designs, HVAC&R Research 2010; 16(5): 707-728.

[22] Cressie, N., Statistics for Spatial Data, 1993; John Wiley & Sons, New York.

[23] Deb, K. Multi-objective Optimization using Evolutionary Algorithms, 2001; John Wiley & Sons, New York.

[24] Tancabel, J., Aute, V., & Ling, J. Optimization of R290 Heat Exchangers using High-Performance, Non-round Tubes. 14th IIR-Gustav Lorentzen Conference on Natural Refrigerants; 2020.

[25] Private communications, 2019.

[26] Tiller, P.L., The NURBS Book. 1995; Springer, New York.

[27] Radermacher, R. Design and Manufacturing of High Performance, Reduced Charge Heat Exchangers (HPRC-HX), 2019; United States Department of Energy BTO Peer Review.

[28] ANSYS, Inc. Ansys® GAMBIT, Release 2.4.6, 2018.

[29] ANSYS, Inc. Ansys® Academic Research Fluent, Release 18.0, 2018.

[30] Shih, T.H., Zhu, J., & Lumley, J.L., A new Reynolds stress algebraic equation model, Computer Methods in Applied Mechanics and Engineering, 1995; 125(1-4): 287-302.

[31] Bergman, T.L., Incropera, F.P., DeWitt, D.P., & Lavine, A.S. Fundamentals of Heat and Mass Transfer – 7th Edition. 2011; John Wiley & Sons: Hoboken, NJ.

[32] Roache, P.J., Quantification of Uncertainty in Computational Fluid Dynamics, Annual Review of Fluid Mechanics, 1997; 29(1): 123-160.

[33] ASME, Standard for Verification and Validation in Computational Fluid Dynamics and Heat Transfer, ASME V&V 20-2009, 2009; American Society of Mechanical Engineers: New York, New York, USA.

[34] Oberkampf, W., Roy, C., Verification and Validation in Scientific Computing, 2010; Cambridge University Press, Cambridge, UK.

[35] Roy, C., Oberkampf, W., A Comprehensive Framework for Verification, Validation, and Uncertainty Quantification in Scientific Computing. Computer Methods in Applied Mechanics and Engineering. 2011; 200(25): 2131–2144.

[36] McKay, M.D., Beckman, R.J., & Conover, W.J., Comparison of Three Methods for Selecting Values of Input Variables in the Analysis of Output from a Computer Code, Technometrics, 1979; 21(2): 239-245.

[37] Hamad, H., A New Metric for Measuring Metamodels Quality-of-Fit for Deterministic Simulations. 38th conference on Winter Simulation, 2006; 882-888: Monterey, California, USA.

[38] Jiang, H., Aute, V., & Radermacher, R., CoilDesigner: A General Purpose Simulation and Design Tool for Air-to-Refrigerant Heat Exchangers, International Journal of Heat and Mass Transfer, 2006; 29(4): 601-610.

[39] Lemmon, E.W., Bell, I.H., Huber, M.L., & McLinden, M.O. NIST Standard Reference Database 23: Reference Fluid Thermodynamic and Transport Properties-REFPROP, Version 10.0, 2018; National Institute of Standards and Technology, Standard Reference Data Program, Gaithersburg, MD.

[40] Aute, V. and Radermacher, R. Standardized polynomials for fast evaluation of refrigerant thermophysical properties. 15th International Refrigeration and Air Conditioning Conference, Purdue University, 2014; Paper 1499: West Lafayette, Indiana, USA.

[41] Gnielinski, V. New equations for heat and mass transfer in turbulent pipe and channel flow. International Chemical Engineering, 1976;16(2): 359-368.

[42] Churchill, S.W. Friction-factor equation spans all fluid-flow regimes. Chemical Engineering, 1977: 91–92.

[43] Shah, M.M. Improved correlation for heat transfer during condensation in conventional and mini/micro channels. International Journal of Refrigeration, 2019; 98: 222-237.

[44] Xu, Y. and Fang, X. A new correlation of two-phase frictional pressure drop for condensing flow in pipes. Nuclear Engineering and Design, 2013; 263: 87-96.